Development of a Variable Stiffness Mechanism with a Linear Output for Exosuit Integration

Verburg, Tim; Joshi, Sagar; Seth, Ajay; Della Santina, Cosimo

DOI
10.1109/BioRob60516.2024.10719772

Publication date
2024

Document Version
Final published version

Published in
Proceedings of the 10th IEEE RAS/EMBS International Conference for Biomedical Robotics and Biomechatronics, BioRob 2024

2024 10th IEEE RAS/EMBS International Conference for
Biomedical Robotics and Biomechatronics (BioRob)
1-4 September 2024. Heidelberg, Germany

Development of a Variable Stiffness Mechanism with a Linear Output for Exosuit Integration

Tim Verburg[1], Sagar Joshi[1], Ajay Seth[2], Cosimo Della Santina[3]

***Abstract*— People suffering from conditions affecting their activities of daily living and those who do straining repetitive tasks could be assisted using supportive devices. These devices have generally been stiff in design, with more recent advances exploring soft suits, removing the need for heavier structural components. These supportive devices are often fitted with rigid actuators that lack inherent compliance and rely on feedback to regulate the assistive force. Compl iant actuators able to control stiffness and pretension have only been applied in rigid assistive devices with these devices being designed for controllable stiffness in rotation and not linear motion. This work briefly presents the results of a user study on the effects of a compliant actuator in a soft supportive device for arm flexion, the development and testing of a variable linear stiffness mechanism for a linear motion capable of controlling the stiffness and equilibrium position, and the integration of said actuator in an exosuit.**

I. Introduction

From patients with limited strength and mobility to workers performing repetitive lifting tasks, supportive devices could alleviate some of their problems [1], [2]. With devices being designed to assist in walking [3], [4], to others focusing on supporting the upper limbs [5], [6], a wide variety of applications are covered. These supportive devices have traditionally been rigid with more recent designs utilizing fabrics to create exosuits as opposed to exoskeletons, removing the need for heavy structural components prone to parasitic forces [7]. Most assistive devices use rigid actuation strategies that do not allow for inherent compliance and rely on sensing and control to vary the assistive force [8]. The application of actuators with mechanical compliance has been mostly restricted to rigid assistive devices [9] with no solution existing that combines an exosuit with an actuator with controllable stiffness and pretension. Most of the variable stiffness solutions used are additionally designed for a joint [10]–[14] as opposed to a linear motion [15]–[17], with the latter lacking either a linear stiffness output, controllable stiffness and pretension, or the capability to set the mechanism at infinite or zero stiffness.

The need for a variable stiffness actuator stems from our user study studying the efficacy of the passive-adaptive exosuit that was created by augmenting the suit from [18], which is designed to assist the right shoulder flexion by pretensioning a spring as seen in figure 1, with a motor to pretension a spring on the upper arm. To highlight the efficacy, a muscle effort reduction as a percentage of the maximum voluntary contraction of 3.03%, 2.4%, 1.56%, and 2.13% were observed for the deltoid anterior, deltoid mid, deltoid posterior, and the trapezius respectively for the fourth experiment with and without the exosuit with an experienced user. Further reductions in muscle effort were theorized to be possible with the addition of a variable stiffness mechanism due to greater control over the provided support, thus forming the basis for this work.

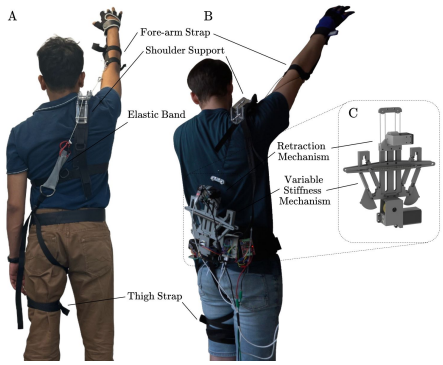

Fig. 1: (A) The original entirely passive exosuit utilizing an elastic band [18]. (B) The final integrated exosuit with the variable stiffness mechanism. (C) The final version of the variable stiffness mechanism.

The goal of this work is to meet the need for a variable stiffness solution for a linear motion to be integrated into an exosuit filling two academic gaps, (i) a linear motion variable stiffness mechanism with a linear stiffness output capable of both equilibrium and stiffness control, and (ii) using a variable stiffness mechanism with equilibrium and stiffness control in an exosuit. This work focuses on the first part and will present the integrated system as a proof of concept. The design parameters will be defined in section II, after which the design and working principle will be explained in section III. This design is then subject to a series of experiments in section IV, to validate the functionality of the mechanism and highlight areas of improvement. Finally, section VI will draw the final conclusions and discuss the future possibilities and improvements.

II. Design Specifications

The mechanism itself will sit at a preferred location on the lower back, where it proved a convenient location for

[1] T. Verburg and S. Joshi are with the Cognitive Robotics Department, Delft University of Technology, Mekelweg 2, 2628CD, Delft, The Netherlands tim.verburg@hotmail.com & sagajosh@gmail.com

[2] A. Seth is with the BioMechanical Engineering department, Delft University of Technology, Mekelweg 2, 2628 CD Delft, Netherlands b.d.researcher@ieee.org

[3] C. Della Santina is with the Cognitive Robotics department, Delft University of Technology, Mekelweg 2, 2628 CD Delft, Netherlands. He is also with the Institute of Robotics and Mechatronics, German Aerospace Center (DLR), 82234 Weßling, Germany C.DellaSantina@tudelft.nl

donning and doffing the suit as well as bearing the load of the mechanism when attached to a wide belt as seen in figure 1.

A. Functional Requirements

1) Maximum Tension: The mechanism is designed to function with two springs in parallel with a total stiffness of $425\,\mathrm{N/m}$. The desired pretension length of the spring measured during the user study was up to $231\,\mathrm{mm}$ with the maximum measured deflection of the spring being $163\,\mathrm{mm}$. This combined with the previously mentioned spring stiffness results in a maximum force of $69\,\mathrm{N}$ measured during the user study. Considering a safety margin of at least 10% the designed for maximum force is chosen to be $80\,\mathrm{N}$.

2) Stiffness Range: A stiffness of $425\,\mathrm{N/m}$ was chosen due to a higher stiffness requiring less pretensioning of the spring. The mechanism should at least be capable of reaching the stiffness used in the user study to allow for a conclusive comparison while preferably also being able to become completely compliant. Being able to set the mechanism to an infinite stiffness might also be desired as it would allow the user to hold their arm stationary with the mechanism bearing the majority of the load. Therefore, the desired stiffness range thus will be from $0\,\mathrm{N/m}$ to $\infty\ \mathrm{N/m}$.

3) Retraction Distance: As previously mentioned, the highest desired pretension distance during the user study was $231\,\mathrm{mm}$. To obtain an estimate of the distance the mechanism has to actuate to move the equilibrium location of the output, a measurement was done with a fully raised arm and compared to a fully lowered arm. Measuring on an $180\,\mathrm{cm}$ male resulted in a measured distance of approximately $160\,\mathrm{mm}$. Considering taller people, or those with larger shoulders, a maximum retraction distance of $200\,\mathrm{mm}$ was selected. Noteworthy is that the $160\,\mathrm{mm}$ retraction corresponds to a 180-degree rotation of the arm, illustrating the large effect a small displacement of the mechanism has on the arm angle.

B. Performance Criteria

1) Speed: The mechanism should be able to actuate the previously mentioned retraction distance in 2 seconds or less as this is approximately the time it takes to lift the arm from minimum to maximum elevation. A stiffness change from $0\,\mathrm{N/m}$ to $\infty\ \mathrm{N/m}$ should also be able to be done within this same time window.

2) Weight: The weight of a portable solution is crucial for the comfort of the user and should thus be kept to a minimum or allocated such as to optimize for the comfort of the wearer.

3) Power Consumption: Another crucial metric in a portable solution is power consumption as this will, combined with the desired operating time, result in the required battery capacity of a system equipped with the variable stiffness actuator, adding additional weight. The average power consumption of the system should therefore be kept to a minimum.

4) Inertia: The inertia of the mechanism should be as low as possible to maximize the transparency to the user and minimally affect the bandwidth of the motions.

C. Additional Criteria

The mechanism would preferably be affordable to build to allow anyone to easily recreate it as the linear variable stiffness mechanism can be used in other settings also. Additionally, the design should be easily manufacturable with limited resources as this would further promote easy replication and improvement of the design both during the design phase and beyond.

Furthermore, the center of mass of the mechanism should be kept as close to the back of the wearer as possible to minimize the generated moment due to gravity, improving the comfort.

III. System Design

Most of the variable stiffness designs found in the literature phase are for rotary joints with only one being designed for a linear motion but still applied in a rotary joint using a pulley [19]. With that in mind, a point of reference remains valuable to compare existing variable stiffness solutions for rotary joints to understand the capabilities of current solutions.

TABLE I: Exemplary variable stiffness joints

Name	VS-Joint [10]	DLR FSJ [11]	vsaUT-II [12]	AwAS-II [13]
Max.Torque	160 Nm	67 Nm	60 Nm	80 Nm
Max. Stiff.	55 Nm/deg	83.7 Nm/deg	16.5 Nm/deg	∞ N/deg
Zero Stiff.	✗	✗	✓	✓
Max. Defl.	$\pm 14°$	$\pm 15°$	$\pm 20°$	$\pm 17°$
Weight	1.4 kg	1.41 kg	2.5 kg	1.1 kg

It is challenging to compare these systems to the to-be-designed system due to the target application being linear as opposed to rotation and would benefit from a greater deflection at a lower stiffness. Noteworthy, however, is the fact that only two of these actuators have the capability to be completely compliant, namely the vsaUT-II actuator by [12] and the AwAS-II actuator by [13], with only the latter having the ability to also become completely rigid. A further limitation within these designs is the limited deflection angle of the joints, which for their designed purpose is most likely ideal, but would translate poorly if used in a linear mechanism using a pulley due to the previously mentioned preference for greater deflections at a lower stiffness.

A. Variable Stiffness

The variable stiffness mechanism is designed to adhere to the requirements set in section II. The specific application of the exosuit allows freedom due to the absence of the usual constraint given to the variable stiffness mechanisms seen in the literature, namely that it has to be as compact as possible to fit in a joint. The variable stiffness mechanism will be placed on the lower back where there is ample space in the plane parallel to the back. As mentioned in section II-C, the center of mass should be kept as close to the back as possible which can be achieved by minimizing the mechanism thickness.

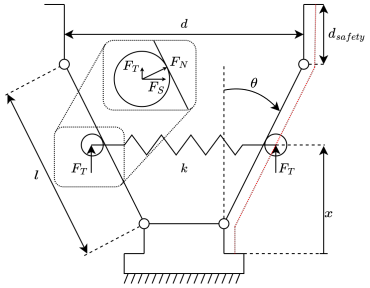

Fig. 2: Concept of the variable stiffness mechanism with the angle θ of the slope as the controlled variable. Two bearings roll over the surface along the red-dotted path and exert a normal force F_N on the surface which can be decomposed into F_S and F_T at a displacement of x. Between the two bearings, a spring with stiffness k_s is placed that extends as the bearings further separate, increasing F_S and thus F_T. The distance d_{safety} has been added as a short piece that has an output stiffness of only $4.4\,\text{N/m}$ in the event that there is an excessive amount of force on the mechanism in the lower operating stiffness range.

The working principle of the developed concept can be seen in figure 2, where the angle θ can be adjusted using a motor. The system has two bearings that roll over the surface and follow the red-dotted line with each bearing a tension F_T at a displacement of x. As the slope increases, the rate at which the spring extends with an increase of displacement x also increases and thus the output stiffness increases. The mechanism effectively multiplies the stiffness of the spring using mechanical advantage, and can thus be categorized under the structure-based variable stiffness mechanisms as discussed in section I.

After conceptualizing the functionality of this mechanism, a design was found that utilized a similar working principle to obtain a nonlinear stiffness by having the bearings roll over a nonlinear surface, and in doing so map linear springs to any nonlinear spring output for use in an antagonistic-based variable stiffness mechanism [20]. The main difference between the presented concept and the found design is that the concept will be able to adjust the spring characteristic during operation and the found design has no such ability as the profile has to be manufactured in advance. The spring force is determined by $F_S = k \cdot s = k_s 2x \tan(\theta)$ from which follows the tension force

$$F_T = \tan(\theta) F_S = k_s 2x \tan(\theta)^2. \tag{1}$$

This relation can then be used to find the relation between the input stiffness and output stiffness as well as the desired arm angle to attain a certain output stiffness using $F_{\text{Total}} = 2F_T = k_s 4x \tan(\theta)^2$ from which follows

$$k_{\text{output}} = \frac{F_{\text{Total}}}{x} = k_s 4 \tan(\theta)^2, \tag{2}$$

$$\theta = \text{atan2}(\sqrt{k_{\text{output}}}, \sqrt{4k_s}). \tag{3}$$

In the configuration where θ is zero, the mechanism will have an output stiffness of $0\,\text{N/m}$ as there is no extension of the spring. Then, as θ increases, the output stiffness will increase with x and θ as defined by equation 2. The top plot in figure 3 illustrates the output stiffness k_o as a function of θ for three available spring stiffnesses. This stiffness would continue to increase until infinity at $\theta = 0.5\pi$.

As the mechanism is able to theoretically create any output stiffness from an input stiffness, the spring stiffness k_s needs to be chosen based on the desired granularity of the output stiffness and the maximum output deflection. A lower spring stiffness allows for greater control in the lower stiffness range however also requires a greater angle θ to obtain higher output stiffnesses and thus limits the possible extension of the mechanism in the higher stiffness range. At greater angles of θ the maximum range over which the mechanism can operate decreases as can be seen in the bottom plot in figure 3, which illustrates the relation between θ and the maximum possible extension of the mechanism $x_{\max}$.

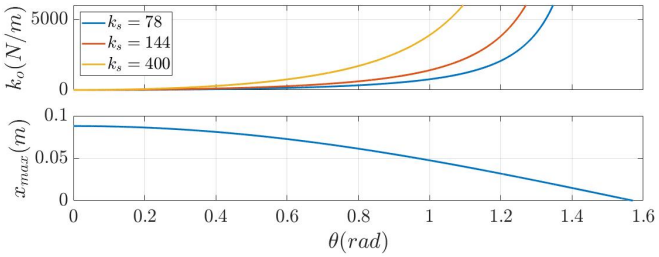

Fig. 3: The top plot illustrates the relation between the spring stiffness k_s, θ, and the output stiffness k_o. The bottom plot gives the relation between the spring stiffness θ and the maximum extension of the mechanism $x_{\max}$.

A spring stiffness of $144\,\text{N/m}$, consisting of two $72\,\text{N/m}$ springs in parallel, was chosen from the set of available springs as the lower stiffness would allow for greater control in the lower stiffness range while also having an outside diameter of $12.5\,\text{mm}$ with a rest length of $76\,\text{mm}$, making it ideal for the mechanism to remain thin while increasing in width along the back.

The addition of the $4.4\,\text{N/m}$ section of length d_{safety} was added based on experience from the user study discussed in section I, as occasionally, the wearer would experience a higher than comfortable tension and thus would be forced to lift the arm practically vertical. The reason the stiffness is nonzero is that the low stiffness still generates enough force to reset the mechanism. The distance d_{safety} would theoretically allow for the mechanism to be overpowered as long as it would be operating a stiffness range that would not require an impossible amount of force. The distance d_{safety} can be quite short since a small displacement would have a large effect on the arm angle as discussed in II-A.3.

Figure 4 illustrates the relation between the output stiffness and the required force to trigger the safety with the mechanism having an arm length l of $88\,\text{mm}$. For the previously mentioned spring stiffness of $144\,\text{N/m}$ the required force at an output stiffness of $2000\,\text{N/m}$ would theoretically be $83.2\,\text{N}$. This is slightly higher than the maximum force, as set in II-A.1, ensuring the maximum force can still be achieved. A greater force would trigger the safety, which could be modified by altering the length of the arms or the desired output stiffness. The addition of the safety does complicate

the design somewhat since it requires the design to function as a parallelogram to ensure the stiffness at the end remains $4.4\,\mathrm{N/m}$.

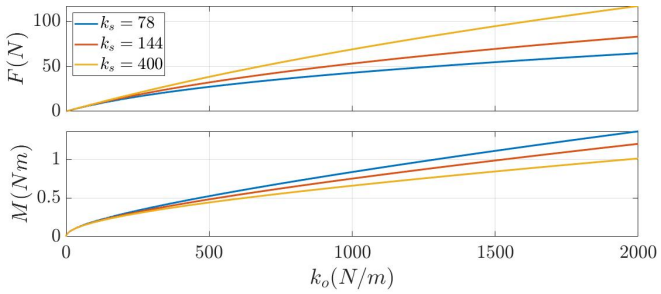

Fig. 4: The top plot illustrates the relation between the output spring stiffness k_o, and the required force to trigger the safety F. The bottom plot shows the relation between the output spring stiffness k_o, and the required moment M to actuate one arm at the maximum chosen arm length of $88\,\mathrm{mm}$.

The maximum required moment M to actuate with an arm length of $88\,\mathrm{mm}$ as a function of the output stiffness relation k_o can be seen in the bottom plot of figure 4. At an output stiffness k_o of $2000\,\mathrm{N/m}$, the maximum required moment to actuate one arm is $1.2\,\mathrm{Nm}$, thus the total moment required to actuate both arms is $2.4\,\mathrm{Nm}$. The system uses a motor that was already available in combination with a worm wheel to make the system non-back-drivable and thus reduce the energy consumption of the system. The motor has a rated operating torque of $0.125\,\mathrm{Nm}$ with a peak torque output of $0.38\,\mathrm{Nm}$ and is combined with an also already available worm wheel that has a 90:1 reduction ratio. Furthermore, the axis of the worm wheel is fitted with a magnet and an as5600 hall sensor to provide feedback to the controller.

The system, additionally, has another transmission ratio due to the differing diameters of the pulley on the worm wheel being $32.3\,\mathrm{mm}$ and the diameter of the pulley on the arm being $68\,\mathrm{mm}$ as seen in figure 5a, resulting in a ratio of 1.98:1. This subsequently leads to a total reduction ratio of 178.2:1, leading to a maximum peak operating torque of $22.275\,\mathrm{Nm}$. This is many times greater than the required torque at an output stiffness k_o of $2000\,\mathrm{N/m}$, and would theoretically allow the system to actuate at a maximum displacement at a stiffness of $40\,000\,\mathrm{N/m}$. The reason for using wires rather than direct gearing is that it would allow for easy symmetrical actuation due to the absence of play in gears and improve efficiency as there are no sliding contacts.

With the previously mentioned total reduction ratio of 178.2:1 and the nominal speed of the motor being $4000\,\mathrm{rpm}$ the motor could theoretically actuate $2\,\mathrm{s}\cdot 360\,\mathrm{deg}\cdot\frac{4000\,\mathrm{rpm}}{60\,\mathrm{s}\cdot 178.2} = 269.36\,\mathrm{deg}$ in two seconds. This would satisfy the performance criteria set in section II-B.1.

B. Rest Length Adjustment

Now the variable stiffness element of the mechanism has been designed, a mechanism needs to be designed to reduce the cable length. The biggest challenge is creating a design that integrates well with the variable stiffness mechanism while adhering to the requirements. To this extent, to maintain the possible deflection of the integrated solution, the existing cable layout has to be modified to maintain the 1:1 movement of the output to the mechanism using a pulley as seen in figure 5a and figure 5b.

The first iteration of the design can be seen in figure 5b where a servo is used to rotate a pulley to spool the cable. Due to the cable layout, the cable retraction mechanism has to actuate twice the distance for the desired output retraction distance. At the maximum force set in II-A.1 and with a pulley diameter of $40\,\mathrm{mm}$ the required torque is $0.8\,\mathrm{Nm}$ without losses. A Dynamixel XM-430-r was chosen as it was available, easy to use, having a rated stall torque $3.0\,\mathrm{Nm}$ at $12\,\mathrm{V}$, and allowing for continuous rotation. It has to be emphasized that this is but the first iteration of the design and currently does adhere to the performance requirement as set in II-B.1, as with a $40\,\mathrm{mm}$ pulley, the system would need $2.48\,\mathrm{s}$ to actuate $0.2\,\mathrm{m}$ without load. The pulley diameter could be increased but doing so would result in a lower output force, which was prioritized for this design iteration. The current design requires the servo to continuously actuate and thus does not optimize the performance requirement as set in II-B.3. Ideally, a similar non-backlash system, such as a worm wheel, would be used to allow for minimal actuation. The design could be effectively improved by using a different actuation solution that would also allow for continuous rotation while having a higher rated torque while including a non-backlash solution as will be further discussed in section VI.

C. Integrated Design

The last step of the design process integrates the variable stiffness mechanism with the cable retraction mechanism. The variable stiffness mechanism was designed first, with the cable retraction mechanism being designed with that in mind, connecting to the guide structure using a set of bolts as illustrated in figure 5b. The design including the control electronics weighs $1224\,\mathrm{g}$ which is comparable to the designs presented in table I. A large part of the weight is due to the stiffness actuation motor weighing $0.45\,\mathrm{kg}$, and as previously mentioned was chosen for availability and will be further discussed in section VI.

D. Control

The chosen controller is a PI controller as the target application is reference tracking, allowing for a minimal steady-state error. A block diagram of the controller can be seen in figure 6. The controller was manually tuned through trial and error, likely limiting the performance of the controller but considered sufficient for the proof-of-concept. The reference angle of the worm wheel r is set based on the desired stiffness as defined in equation 3 that is derived from equation 2. The error e between the measured angle of the worm wheel y and r is then used as input of the PI controller which outputs the motor velocity that accepts a range from 0, being zero velocity, to 4095, being the maximum motor velocity. The integral in the PI controller is saturated at a value of ± 250 to allow for fast changes in direction and little overshoot with the control input bounded to a value of 1500

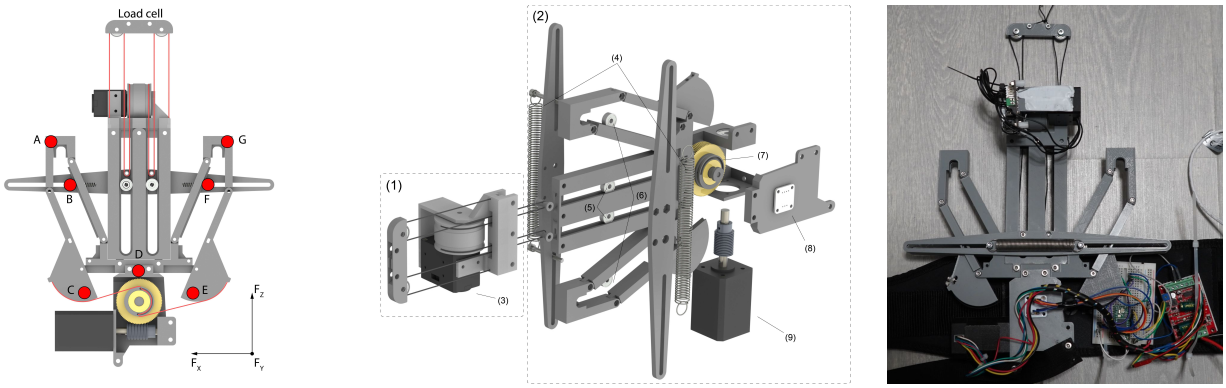

(a) (b) (c)

Fig. 5: (a) A top-down section view illustrating the cable routing of the mechanism in red and the mechanism of actuation for the arms and marker placement on the mechanism for the experiments. (b) An exploded view of the mechanism highlighting the most important components. (1) The retraction mechanism mainly consists of (3) the retraction servo. (2) The variable stiffness mechanism with (4) the two springs, (5) the guiding roller bearings, (6) the roller bearings for the springs, (7) the worm wheel with integrated pulley, (8) the hall effect sensor, and lastly (9) the motor for the stiffness actuation. (c) picture of the physical prototype.

to limit the speed of the system which after further testing could be increased for increased system responsiveness.

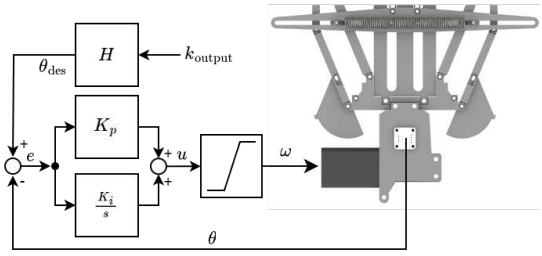

Fig. 6: Block diagram of the system with k_{output} being the desired output stiffness is transformed to a resulting desired motor angle θ_{des} using equation 3 in combination with the transmission ratio between the arms and the worm wheel. The error e between the desired angle θ_{des} and the measured angle of the worm wheel θ, is used as an input in the PI controller. u is the control input determined by the PI controller which is the motor velocity from stationary being 0 to the maximum velocity being 4095 and is bounded to limit the speed of the system.

IV. Experiments

The following experiments were performed throughout the iteration process to debug and validate the code and mechanical design: (1) Repeatability, (2) Constant displacement, (3) Constant force, (4) Limit test, (5) Performance analysis, and (6) Bending analysis. The goals of the experiments were as follows: (1) To measure the consistency of the mechanism, (2) to test the mechanism's ability to change stiffness at a constant output displacement, (3) to test the mechanism's ability to maintain a set force while changing pretension, (4) to find the limits of the mechanism, (5) to measure the performance criteria, and (6) to measure the mechanical deflection of the mechanism under load. Notably, the two design objectives inertia and power consumption will not be measured as the found design was deemed subject to change.

A. Methodology

An OptiTrack system sampled at 200 Hz with the data from the Teensy microcontroller streaming at 10 Hz over serial communication. The mechanism is turned on and calibrated to the zero stiffness position based on observed tension in the cables connecting the motor pulley to the arms, after which the control is enabled and the OptiTrack system recording starts. Depending on the experiment, the automated or manual testing then commences. After the experiment finishes, the Teensy data is saved with the OptiTrack recording stopped. The data is aligned and trimmed to the same length after which the Teensy data is supersampled to match the sampling frequency of the OptiTrack recording allowing for easy data analysis using Matlab.

B. Repeatability

To validate the repeatability of setting the mechanism stiffness a test was performed where the mechanism stiffness would increase with $50\,\mathrm{N/m}$ increments and be pretensioned with a distance of Δx_p m, as defined by $\Delta x_p = 2 \cdot 0.088\cos(\theta)$. This was done over a range from $50\,\mathrm{N/m}$ to $2000\,\mathrm{N/m}$ as this was found to be the range in which the retraction mechanism was able to actuate consistently. This test was performed 13 times without adjusting the output position but with re-calibration of the initial position after each experiment. Some slack in the output cable was observed in the starting position meaning the mechanism would in reality actuate slightly less than Δx_p m which was compensated for using the measured position of the tracking markers as seen in figure 5a. Due to the complete data collection, various methods of calculating the resulting stiffness are possible of which two were chosen for their logic and hypothesized quality of data.

1) Calculated Stiffness Using Measured Force: The first method uses the force of the load cell in combination with the measured displacement of the spring mechanism over the Z-axis as defined in figure 5a, of which the results can be seen in figure 7. Figure 7 also illustrates the error between the desired stiffness and the calculated stiffness, showing an average stiffness error over all trials of this experiment of $-237.018\,\mathrm{N/m}$, meaning the mechanism was on average less

stiff than desired. Furthermore, an increased variance can be seen as the desired output stiffness increases.

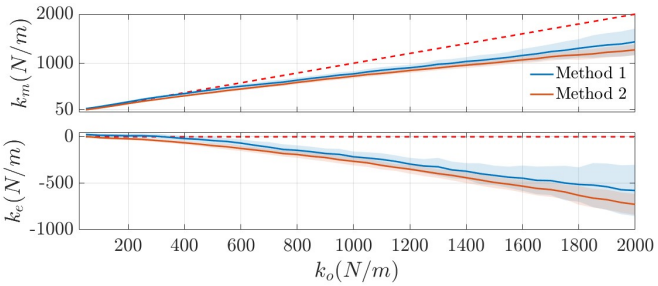

Fig. 7: The top plot shows the relation between the measured output stiffness k_m and the target output stiffness k_o with method 1 being calculated using the measured tension and the displacement of the spring in the Z direction as defined in figure 5a and method 2 being calculated using the measured extension of the spring, the motor angle, the force relation in equation 1, . The bottom plot shows the stiffness error k_e between the measured stiffness and the desired output stiffness.

2) Calculated Stiffness Using Measured Spring Extension: The second method uses the two markers, marker B and F in figure 5a, on the springs to measure the spring extension by taking the Euclidean distance between the two points, multiplying that by the total spring stiffness of $144\,\mathrm{N/m}$, and using the relation in equation 1 to calculate the resulting output force. This force is divided by the displacement of the spring in the Z-axis, like in the other method, and results in an output stiffness as can be seen in figure 7. The average stiffness error k_e over all trials in this experiment was found to be $-306\,\mathrm{N/m}$, indicating the mechanism was on average over all the experiments below the desired stiffness using this method.

3) Comparison Of Methods: Both methods show the effect of the system compliance can be seen in the figures as the error grows larger due to the higher angle and force, further studied in section IV-G. Effectively, this would equate to two springs in series, that being the actual springs and the mechanism itself, leading to a lower output stiffness. Additionally, the force measurement used in the first method seemed to fluctuate, making conclusions increasingly challenging. The range of the error is smaller in the second method with a maximum standard deviation of $266.94\,\mathrm{N/m}$, as opposed to from $308.79\,\mathrm{N/m}$ for the first method. The variable stiffness devices mentioned in chapter III do not mention the stiffness errors and as such the error cannot be compared to existing devices in literature. The second method was chosen as the default method based on the observed inconsistency of the load cell data and the lower variance of the collected data. The second method should better reflect the actual state of the system as the physical spring extension is used. A counter-argument to the second method is that it negates the effects of friction in the system which would be better represented by the load cell data.

C. Constant Displacement

The constant displacement experiment illustrates the ability of the mechanism to change the output stiffness for a constant displacement of the system. The output of the system was fixed to a rigid frame with the mechanism placed at a displacement of $0.03\,\mathrm{m}$. This would allow for the exploration of a large range of stiffnesses but does prevent the mechanism from reaching an infinite stiffness as this would require the output to move due to the radius of the bearing as discussed in IV-D. The results are illustrated in figure 8. During the experiment, it was observed that the mechanism was more capable of reaching the desired stiffness by first returning to the zero stiffness configuration. The error between the desired stiffness and the measured stiffness increases with an increasing desired stiffness. The error was lower for the same stiffness if the mechanism was first reset to the zero stiffness configuration, as evident by the lower error in figure 8. The highest measured tension using the loadcell was $83.10\,\mathrm{N}$, at which point the mechanism was unable to further actuate with the current controller and motor used to control the mechanism stiffness. The calculated force based on the method from IV-B.2, resulted in a maximum force of $99.53\,\mathrm{N}$.

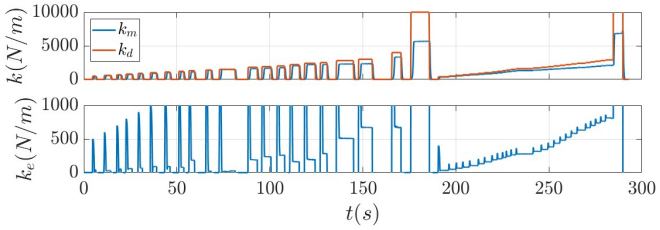

Fig. 8: The top plot shows the desired output stiffness k_d and the measured output stiffness k_m, as per the method in IV-B.2, over time for the constant displacement experiment. The bottom plot shows the error between the two over time.

D. Constant Force

To validate the ability of the mechanism to output a constant force, the mechanism has to counteract the change in force due to the stiffness change. As the stiffness, and thus the angle θ, is increased, there is a following displacement Δx_θ due to the offset of the center of the bearing with respect to the rolling surface. This relation is defined by $\Delta x_\theta = r_{bearing}(\sin(\theta_1) - \sin(\theta_2))$, with θ_1 and θ_2 being the angles at a stiffness of k_1 and k_2 respectively. From this the relationship between the required actuation distance Δx can be determined using $xk_{output,1} = (x + \Delta x + \Delta x_\theta)k_{output,2}$ from which follows $\Delta x = \frac{xk_{output,1}}{k_{output,2}} - x - \Delta x_\theta$.

The experiment was performed with the mechanism being set at an initial displacement of $0.03\,\mathrm{m}$ with an output stiffness of $400\,\mathrm{N/m}$ and then decreased with increments of $25\,\mathrm{N/m}$ to the final stiffness of $150\,\mathrm{N/m}$.A lower stiffness would result in the mechanism safety triggering, as the required mechanism pretension would be greater than the actuation range. The results can be seen in figure 9, where the measured starting force was $11.85\,\mathrm{N}$ and ending with $8.99\,\mathrm{N}$ with a mean of $10.22\,\mathrm{N}$ and a standard deviation of $0.853\,\mathrm{N}$.

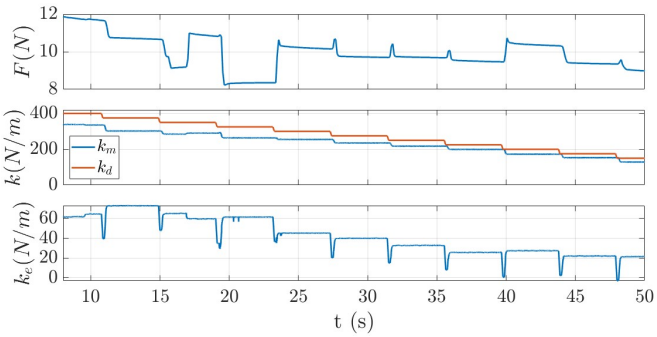

Fig. 9: The top plot shows the measured force from the loadcell F during the constant force experiment. The middle plot shows the desired output stiffness k_d and the measured output stiffness k_m as per the method described in IV-B.2. The bottom plot shows the error between k_d and k_m.

E. Limit Testing

To find the actual limits of the device including the pretensioning mechanism, a test was performed that would incrementally increase the mechanism stiffness and maximally pretension the mechanism with a distance of Δx_p m, as defined by $\Delta x_p = 2 \cdot 0.088 \cos(\theta)$. The results can be seen in figure 10. The stiffness at which the mechanism became unable to further actuate was at a desired stiffness of $2700\,\mathrm{N/m}$ with a measured stiffness of $1933\,\mathrm{N/m}$ at a peak force of $51.58\,\mathrm{N}$ due to the error in the servo position being above the predefined limit and as such indicates that the motor is underpowered and should be replaced with a system similar to the stiffness control mechanism while being also being capable of higher cable tensions as previously mentioned in section **??**. This limit could be increased at the expense of the output accuracy. With a force of $51.58\,\mathrm{N}$, it does not satisfy the requirement set in II-A.1 and should be further iterated upon as previously mentioned in section III-B.

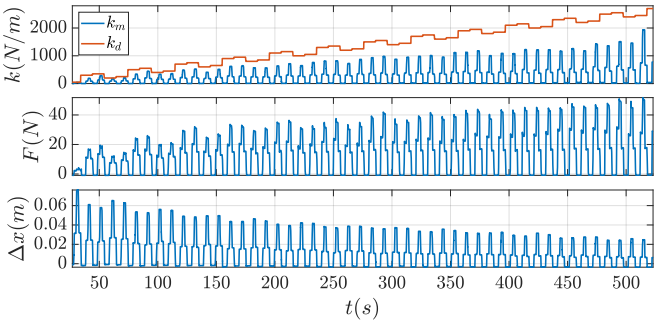

Fig. 10: The results of the limit test experiment.

F. Performance analysis

To validate some of the performance criteria, a test was done to find the capabilities of the mechanism to change the output stiffness from $0\,\mathrm{N/m}$ to $\infty\ \mathrm{N/m}$ and from $0\,\mathrm{N/m}$ to $500\,\mathrm{N/m}$. This experiment was performed without load to test the base capabilities of the mechanism. The mechanism was able to change stiffness from $0\,\mathrm{N/m}$ to $\infty\ \mathrm{N/m}$ in $1.4\,\mathrm{s}$ and from $0\,\mathrm{N/m}$ to $500\,\mathrm{N/m}$ in $1.09\,\mathrm{s}$, thus complying with the requirement set in II-B.1.

G. Deflection under load

Higher-than-expected deflection of the mechanism under load led to the experiments being performed using an OptiTrack system with markers being placed as seen in figure 5a. Besides providing useful data on the spring displacement, it also allows for the measuring of the previously mentioned deflection of the mechanism. This was done by configuring the mechanism with a stiffness of $425\,\mathrm{N/m}$, chosen to match the stiffness from the previous user study. The marker used for the analysis is marker G in figure 5a, as this element was observed to have the highest deflection under load.The results of the experiment can be seen in figure 11, with a maximum deflection of $21\,\mathrm{mm}$ being measured when the mechanism was pulled into the safety and thus had the greatest moment generated. The average equivalent stiffness, meaning the force F divided by the displacement d, was on average $1835\,\mathrm{N/m}$ with a standard deviation of $1260\,\mathrm{N/m}$ and a maximum of $3834\,\mathrm{N/m}$ while under load. The measured deflection is still too high to be considered sufficient and will be further discussed in section VI.

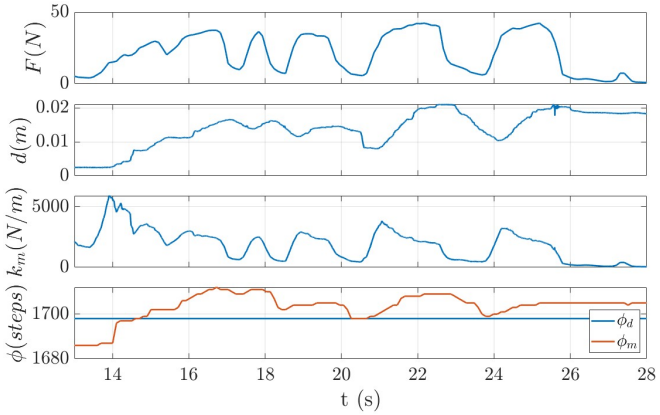

Fig. 11: The results of the bending analysis, from top to bottom: Measured force F, the Euclidean distance of the error of the uppermost marker as seen in figure 5a, the equivalent stiffness based on the measured force and displacement, and the desired motor position ϕ_d and the measured motor position ϕ_m.

V. Proof of Concept

To test the capability of the variable stiffness mechanism as a part of an exosuit, it was integrated into the suit used in the user study discussed in chapter I. The integrated suit fitted to a mannequin can be seen in figures 12.

The suit was also tested to verify the basic working principle and comfort by manually setting the stiffness and pretension as opposed to the biomechanically-aware optimization used in the user study. By pretensioning the system to an equilibrium position where the arm was elevated above the head, and subsequently testing multiple stiffnesses, it was found that there was indeed a significant difference in the stiffness of the mechanism and the effective level of support. The safety was also triggered multiple times

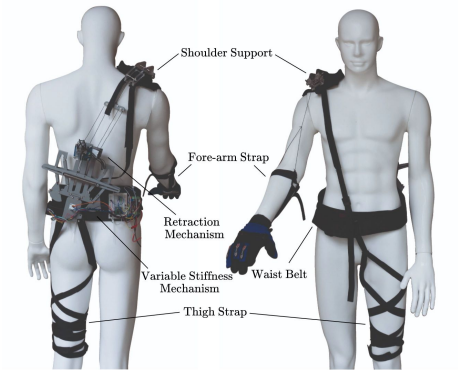

Fig. 12: Picture of the exosuit from the user study equipped with the variable stiffness mechanism fitted to a mannequin.

in the experiment, showing the functionality of the safety mechanism. A frame from the experiment can be seen in figure 1.

VI. Discussion & Conclusion

This work presents a novel variable stiffness mechanism to achieve linear motion variable stiffness with a linear stiffness output capable of both equilibrium and stiffness control and presents a variable stiffness mechanism with equilibrium and stiffness control used in an exosuit. The experiments did indeed validate the working principle and functionality of the design and demonstrated the capabilities of using readily available linear springs and transforming them to any desired linear output stiffness. The stiffness control mechanism was validated to be capable of sustaining the force requirement set, although a relatively high deflection at the end of the arms was measured highlighting a limitation of the current design and the need to further explore possible materials and manufacturing methods while adhering to the set requirements. The current pretensioning mechanism was found to be inadequate and should be improved to be capable of higher forces and should use a power-efficient solution as used in the stiffness control mechanism.

A. Future Work

Integrating the mechanism into the exosuit highlighted limitations in both the exosuit design and the mechanism itself, such as a higher than desired friction in both systems, causing the mechanism to underperform. After addressing this and implementing some if not all of the previously mentioned improvements, a follow-up user study can be performed to test the theorized improved performance of a passive-adaptive variable stiffness exosuit. With the working principle being validated, future iterations can now be made to further optimize the design in performance, volume, and weight.

References

[1] N. Li, T. Yang, P. Yu, J. Chang, L. Zhao, X. Zhao, I. H. Elhajj, N. Xi, and L. Liu, "Bio-inspired upper limb soft exoskeleton to reduce stroke-induced complications," *Bioinspiration & biomimetics*, vol. 13, no. 6, p. 066001, 2018.

[2] I. Pacifico, F. Aprigliano, A. Parri, G. Cannillo, I. Melandri, A. M. Sabatini, F. S. Violante, F. Molteni, F. Giovacchini, N. Vitiello *et al.*, "Evaluation of a spring-loaded upper-limb exoskeleton in cleaning activities," *Applied Ergonomics*, vol. 106, p. 103877, 2023.

[3] P. Slade, M. J. Kochenderfer, S. L. Delp, and S. H. Collins, "Personalizing exoskeleton assistance while walking in the real world," *Nature*, vol. 610, no. 7931, pp. 277–282, 2022.

[4] M. Shepertycky, S. Burton, A. Dickson, Y.-F. Liu, and Q. Li, "Removing energy with an exoskeleton reduces the metabolic cost of walking," *Science*, vol. 372, no. 6545, pp. 957–960, 2021.

[5] B. M. V. Ostuni, T. Caporaso, S. Grazioso, A. Palomba, G. D. Gironimo, and A. Lanzotti, "Preliminary evaluation of an active soft bellow exoskeleton for industrial overhead tasks," in *2023 IEEE International Workshop on Metrology for Industry 4.0 & IoT (MetroInd4.0&IoT)*, 2023, pp. 227–232.

[6] D. Panariello, S. Grazioso, T. Caporaso, G. Di Gironimo, and A. Lanzotti, "A detailed analysis of the most promising concepts of soft wearable robots for upper–limb," in *Design Tools and Methods in Industrial Engineering II: Proceedings of the Second International Conference on Design Tools and Methods in Industrial Engineering, ADM 2021, September 9–10, 2021, Rome, Italy*. Springer, 2022, pp. 71–81.

[7] M. Xiloyannis, R. Alicea, A.-M. Georgarakis, F. L. Haufe, P. Wolf, L. Masia, and R. Riener, "Soft robotic suits: State of the art, core technologies, and open challenges," *IEEE Transactions on Robotics*, vol. 38, no. 3, pp. 1343–1362, 2022.

[8] M. Xiloyannis, D. Chiaradia, A. Frisoli, and L. Masia, "Physiological and kinematic effects of a soft exosuit on arm movements," *J. NeuroEng. Rehabil.*, vol. 16, no. 1, pp. 1–15, Dec. 2019.

[9] S. O. Schrade, K. Dätwyler, M. Stücheli, K. Studer, D.-A. Türk, M. Meboldt, R. Gassert, and O. Lambercy, "Development of varileg, an exoskeleton with variable stiffness actuation: first results and user evaluation from the cybathlon 2016," *Journal of neuroengineering and rehabilitation*, vol. 15, pp. 1–18, 2018.

[10] S. Wolf and G. Hirzinger, "A new variable stiffness design: Matching requirements of the next robot generation," in *2008 IEEE International Conference on Robotics and Automation*. IEEE, 2008, pp. 1741–1746.

[11] S. Wolf, O. Eiberger, and G. Hirzinger, "The dlr fsj: Energy based design of a variable stiffness joint," in *2011 IEEE international conference on robotics and automation*. IEEE, 2011, pp. 5082–5089.

[12] S. S. Groothuis, G. Rusticelli, A. Zucchelli, S. Stramigioli, and R. Carloni, "The vsaut-ii: A novel rotational variable stiffness actuator," in *2012 IEEE International Conference on Robotics and Automation*. IEEE, 2012, pp. 3355–3360.

[13] A. Jafari, N. G. Tsagarakis, and D. G. Caldwell, "Awas-ii: A new actuator with adjustable stiffness based on the novel principle of adaptable pivot point and variable lever ratio," in *2011 IEEE International Conference on Robotics and Automation*. IEEE, 2011, pp. 4638–4643.

[14] Z. Li, S. Bai, O. Madsen, W. Chen, and J. Zhang, "Design, modeling and testing of a compact variable stiffness mechanism for exoskeletons," *Mechanism and Machine Theory*, vol. 151, p. 103905, 2020.

[15] G. Pratt and M. Williamson, "Series elastic actuators," in *Proceedings 1995 IEEE/RSJ International Conference on Intelligent Robots and Systems. Human Robot Interaction and Cooperative Robots*, vol. 1, 1995, pp. 399–406 vol.1.

[16] Y. Shao, W. Zhang, Y. Su, and X. Ding, "Design and optimisation of load-adaptive actuator with variable stiffness for compact ankle exoskeleton," *Mechanism and Machine Theory*, vol. 161, p. 104323, 2021.

[17] I. Gaponov, D. Popov, S. J. Lee, and J.-H. Ryu, "Auxilio: A portable cable-driven exosuit for upper extremity assistance," *Int. J. Control Autom. Syst.*, vol. 15, no. 1, pp. 73–84, Feb. 2017.

[18] S. Joshi, I. Beck, A. Seth, and C. Della Santina, "Minimalistic soft exosuit for assisting the shoulder via biomechanics-aware optimization," in *2022 IEEE-RAS 21st International Conference on Humanoid Robots (Humanoids)*. IEEE, 2022, pp. 667–673.

[19] S. K. Au, H. Herr, J. Weber, and E. C. Martinez-Villalpando, "Powered ankle-foot prosthesis for the improvement of amputee ambulation," in *2007 29th annual international conference of the IEEE engineering in medicine and biology society*. IEEE, 2007, pp. 3020–3026.

[20] S. A. Migliore, E. A. Brown, and S. P. DeWeerth, "Biologically inspired joint stiffness control," in *Proceedings of the 2005 IEEE international conference on robotics and automation*. IEEE, 2005, pp. 4508–4513.